Journal of Catalysis **183,** 267–280 (1999)
Article ID jcat.1999.2398, available online at http://www.idealibrary.com on IDEAL®

Selective Catalytic Reduction of Nitric Oxide by Ammonia over Cu-FAU Catalysts in Oxygen-Rich Atmosphere

Stéphane Kieger,* Gérard Delahay,* Bernard Coq,*,[1] and Bernard Neveu†

*Laboratoire de Matériaux Catalytiques et Catalyse en Chimie Organique, UMR CNRS-ENSCM 5618, ENSCM, 8 rue d'Ecole Normale, 34296 Montpellier Cedex 5, France; and †Grande Paroisse, 12 place de l'Iris, 92062, Paris-La Défense Cedex, France

Received July 28, 1998; revised December 18, 1998; accepted December 21, 1998

The selective catalytic reduction (SCR) of NO (2000 ppm) by NH_3 (2000 ppm) in the presence of oxygen (3%) was carried out on Cu(x)-FAU (x = theoretical exchange degree) catalysts prepared by ion exchange or impregnation and calcined at 773 K. The samples were characterized by UV–visible and IR spectroscopy, temperature-programmed reduction (TPR), temperature-programmed oxidation (TPO), and temperature-programmed desorption (TPD) of NH_3. Ion-exchanged Cu(x)-FAU contains mainly Cu ions located in both supercages and sodalite cavities. In contrast, the impregnated sample contains mainly CuO. Ionic Cu is more active and selective to N_2 than CuO in the temperature range 450–750 K. In contrast, CuO aggregates lead to significant formation of N_2O, with a bell-shaped dependency centered at ca. 540 K. IR spectroscopy and TPD of NH_3 show that the last NH_3 ligand was removed from Cu ions above 550 K. The SCR on Cu ions obeys a $Cu^{2+} \leftrightarrow Cu^{+}$ redox mechanism in which Cu^{2+} is reduced to Cu^{+} by $NO + NH_3$ and Cu^{+} is oxidized to Cu^{2+} by $NO + O_2$, with evolution of N_2 and H_2O. Both reduction and oxidation steps of Cu in the catalytic cycle encompass the reduction of NO in agreement with the SCR of ^{14}NO with $^{15}NH_3$. A new overall SCR reaction below 550 K was proposed: $10NH_3 + 13NO + O_2 \rightarrow 15H_2O + (23/2)N_2$. The active sites below 550 K are formed by several Cu neighbor ions, maybe $[CuOCu]^{2+}$, probably located in the supercages. All Cu ions become active above 600 K. The partial reduction of NO to N_2O occurs at high temperature (>650 K) on exchanged samples. This formation, up to 17% at full NO conversion, is likely to take place on Cu ions located within the sodalite cavities.

Key Words: **selective catalytic reduction; deNO$_x$; Cu-zeolite.**

INTRODUCTION

Besides cars, industrial plants based on combustion processes and nitric acid production emit NO, NO_2, and N_2O in their stack gases. These nitrogen oxides take part in the contribution to photochemical smog, acid rain formation, and the greenhouse effect. To face this problem, the selective catalytic reduction (SCR) of NO_x (NO, NO_2) by NH_3 is by far the most important control technology for the cleanup of flue gases from stationary sources. For several decades, a huge number of catalytic formulations have been evaluated in the SCR of NO_x, which were reviewed in detail (1), as have recent deNO$_x$ SCR commercial catalysts (2). Among these SCR catalysts, two different classes of very efficient materials can be identified: mixed oxides and zeolites. Mixed oxides, of the $V_2O_5/WO_3/TiO_2$ type, are used largely in the treatment of stack gases from power plants (2, 3). Zeolite-based catalysts have received more attention in recent years (4–6).

The SCR mechanism seems now well established on V_2O_5–TiO_2 catalysts (7), but few studies have dealt with these aspects for zeolite-based catalysts. Moreover, the N_2O formation in the process, in particular in the high-temperature region, needs to be carefully considered, due to the future stringent regulations about the emissions of this gas. N_2O is indeed charged to have a very important greenhouse effect.

Recent studies provided definite evidence for the key role of the redox cycle V^{4+}/V^{5+} in the SCR mechanism on V_2O_5–TiO_2 (7). The following overall reaction was proposed on these catalysts:

$$4NO + 4NH_3 + O_2 \rightarrow 4N_2 + 6H_2O. \qquad [1]$$

The same overall reaction was suggested to apply to Cu-zeolite catalysts (8, 9). The relevance of the Cu^{2+}/Cu^{+} redox cycle was also demonstrated, as was the requirement of O_2 to boost the SCR rate (8–11). In the absence of O_2, the rate is low and exhibits a bell-shaped profile when the temperature increases, with a maximum at ca. 400 K (8, 12–14). A surface reaction between strongly adsorbed NH_3 and weakly adsorbed NO was proposed, characterized by a first-order dependence on NO and a zero-order dependence on NH_3 (12). The active site is Cu^{2+} which is reduced to Cu^{+} after the coupling between NO and NH_3. The regeneration of Cu^{+} to Cu^{2+} is very difficult (13), and Mizumoto *et al.* (8) proposed that it occurs through the disproportionation of NO to N_2 and N_2O. Unfortunately, the rate of this reaction decreases when the temperature increases. It could explain the bell-shaped profile observed as a function of reaction temperature (8).

[1] To whom correspondence should be addressed. E-mail: coq@cit.enscm.fr.

0021-9517/99 $30.00

In contrast, oxygen, present in industrial applications, greatly enhances the SCR activity on Cu-zeolites by one or two orders of magnitude (8, 11, 13). On Cu-FAU, Mizumoto *et al.* (8) described a mechanism in which a complex of the form $[Cu(NH_3)_nNO]^{2+}$ gives N_2, H_2O, and Cu^+, which in turn is oxidized to Cu^{2+} with oxygen. They suggested that N_2 comes from the combination of one NO with one NH_3 molecule, and N_2O from three NO molecules (13). The determining role of O_2 for the regeneration of the Cu^{2+} active sites was also put forward as evidence by Ham *et al.* (11) on Cu-MOR. For Komatsu *et al.* (9, 15) N_2 is formed by the interaction of NH_3 with NO_2^-, the latter coming from the oxidation of NO by O_2. This step was claimed to be rate determining (9, 10).

On Cu-MOR, Ham *et al.* (11) and Choi *et al.* (16) proposed two different reaction sites, a metal site (Cu^{2+}) and an acid site (H^+), for which they put forward a dual-site mechanism. In contrast, Komatsu *et al.* (9) suggested for Cu-exchanged H-MFI, H-MOR, and H-FAU catalysts that the active sites were mainly Cu^{2+} paired species, e.g., the dimers $[CuOCu]^{2+}$, in view of the increase in specific activity per Cu site (turnover frequency, TOF) with Cu content. They found Cu-FAU samples more selective to N_2, but much less active than Cu-MFI and Cu-MOR. They concluded that in Cu-FAU some $[CuOCu]^{2+}$ species could be located within unaccessible sites of the framework structure. A possible hindrance to the access of the reactants to $[CuOCu]^{2+}$ species may thus explain the low activity of Cu-FAU. However, several patents claim the use of Cu-FAU as efficient, selective, and stable catalysts for the SCR of NO by NH_3, in particular for application in the treatment of tail gases from acid nitric plants (6). Moreover, recent practice in industrial processes on Cu-FAU has shown that with NH_3/NO molar ratios of about 0.9, 95% of NO_x [$NO_2/(NO + NO_2) \approx 0.5$] removal is nevertheless achieved (17). This observation appears in contradiction with the overall reaction described by Eq. [1].

This work was therefore devoted to study the behavior of Cu-FAU catalysts in the SCR of NO by NH_3 from 300 to 773 K in an O_2-rich atmosphere, with the aim of identifying (i) some aspects of the mechanism and the stoichiometry of the reaction, (ii) the nature of the active sites, and (iii) the origin of N_2O formation. To reach these goals, Cu-FAU catalysts containing either isolated Cu^{n+} ions or CuO aggregates were prepared. They were characterized in detail using TPR/TPO experiments, TPD of NH_3, and FTIR and UV-visible spectroscopies.

EXPERIMENTAL

Preparation of the Catalysts

The Cu-FAU samples prepared for this study were labeled as follow: Cu(x)-FAU, x being the theoretical percentage of Cu exchanged in the zeolite. Cu(x)-FAU with $x = 25$, 37, 56, and 76 were obtained by pouring 2 g Na-FAU (supplied by Süd Chemie, Si/Al $\approx$ 2.55, $S_{BET} \approx 700$ m^2 g^{-1}) into the desired amount of a $Cu(NO_3)_2$ solution ($\approx$0.01 mol dm^{-3}, pH 5) and stirring for 24 h at 298 K. The solid was then separated from the liquid phase by centrifugation, washed with deionized water (30 cm^3), and centrifuged again. The samples were dried for 1 h in an oven at 353 K, and then calcined overnight at 723 K in nitrogen (60 cm^3 min^{-1}) to remove the remaining nitrates. Cu(195)/FAU was prepared by impregnating 2 g of Na-FAU in a 5 cm^3 solution of $Cu(NO_3)_2$ (1.2 g); it was then dried in an oven for 2 h at 353 K and calcined overnight at 723 K in nitrogen. The chemical analyses were performed using plasma atomic absorption spectroscopy at the Service Central d'Analyse du CNRS (Vernaison, France).

Two additional samples, Cu(80)-MFI and Cu(69)-MOR, were prepared according to the same protocol for comparison. The starting materials were H-MFI (Si/Al $\approx$ 27) and H-MOR (Si/Al $\approx$ 7).

Characterization of the Catalysts

The textural properties were determined by adsorption and desorption of N_2 at 77 K, using a Micromeritics ASAP 2000 apparatus. The crystallinity of the samples was checked by XRD on a CGR theta 60 instrument with Cu$K\alpha$ radiation.

The nature of the Cu species was determined by UV–visible spectroscopy. Diffuse reflectance spectra were recorded in the UV–vis region (200–900 nm) with a Perkin Elmer Lambda 14 spectrometer on the as-stored samples. For *in situ* experiments, a self-supported wafer (20 mg) was placed in a dedicated UV cell, activated in He at 773 K, before being contacted with reactant mixtures under various conditions; the spectrum was then recorded at room temperature in the UV–vis–NIR region (200–1100 nm).

The nature, siting, reducibility, and amount of Cu species were estimated by TPR with hydrogen. The experimental setup was derived from that proposed classically (18), and the detection was carried out with a thermal conductivity detector. An aliquot of the sample ($\approx$50 mg) was activated first at 773 K for 1 h in He (ramp = 5 K min^{-1}, flow = 18.6 cm^3 min^{-1}, purity >99.995%) and then cooled to room temperature. The TPR was then started from 298 to 1173 K (ramp = 10 K min^{-1}, flow = 18.6 cm^3 min^{-1}) in a H_2/Ar mixture (3/97, v/v, purity of both gases >99.995%).

The TPO with O_2, NO, or $NO + O_2$ was carried out on some samples pretreated with NH_3. This pretreatment selectively reduces Cu^{2+} to Cu^+ species in Cu-FAU according to previous works (9, 19). The experimental setup was the same as used for the SCR experiments (see later). An aliquot of the sample ($\approx$100 mg) was first reduced with NH_3/He (10/90, v/v, flow = 50 cm^3 min^{-1}, NH_3 purity

>99.95%) at 773 K for about 30 min, flushed with He for 1 h at the same temperature, and then cooled to room temperature in He. The TPO was then started with O_2 (2000 ppm in He, purity of O_2 >99.95%), NO (2000 ppm in He, purity of NO >99.95%), and a $NO + O_2$ mixture (2000 ppm of both in He) at 50 cm^3 min^{-1} from 453 to 773 K (ramp = 5 K min^{-1}).

The nature of the complexes formed by interaction of ammonia with the catalysts was identified by FTIR spectroscopy and TPD of NH_3. TPD profiles of NH_3 were monitored by using the same experimental setup as in the SCR experiments. An aliquot of 20 mg was first treated in He at 773 K and cooled at room temperature, and NH_3/He was then fed to the sample (2500 ppm of NH_3, flow = 50 cm^3 min^{-1}). TPD experiments were conducted from 298 to 773 K in He (ramp = 5 K min^{-1}, flow = 50 cm^3 min^{-1}). TPD was also conducted on a pre-reduced Cu(76)-FAU sample (pretreatment with 2000 ppm of NH_3 at 773 K for 1 h, then cooling to room temperature), which thus contains mainly Cu^+ ions (see above).

For the IR experiments, self-supported wafers (≈20 mg) were placed in a IR cell and activated in N_2 at 773 K for 2 h, then outgassed at 1.3×10^{-3} Pa for 2 h at the same temperature. The cell was cooled to room temperature, and NH_3 was admitted in the cell (13.3 kPa) for about 10 min. The cell was evacuated again at room temperature at 1.3×10^{-3} Pa, to remove weakly bonded NH_3. After evacuation at increasing temperature in steps of 50 K from room temperature to 570 K, the spectra were collected at each stage after cooling back to room temperature, by accumulation of 200 scans with a Nicolet 320 spectrometer (resolution 2 cm^{-1}).

SCR of NO by NH_3

The SCR of NO with NH_3 was studied in a flow reactor operating at atmospheric pressure. Catalyst aliquots (≈20 mg) were activated *in situ* at 773 K in helium (ramp = 10 K min^{-1}, flow = 50 cm^3 min^{-1}) and cooled to room temperature. The reaction gas, a mixture of 2000 ppm NO with 2000 ppm NH_3 and 3% O_2 in helium, was fed to the catalyst. The space velocity was 250,000 h^{-1} (flow = 130 cm^3 min^{-1}). The following protocol was used for the catalytic test: first, a temperature-programmed surface reaction (TPSR) was carried out from 298 to 773 K at 5 K min^{-1} to passivate the catalysts; second, the temperature was decreased back, by step of 25 K and for 1 h, to determine the catalytic behavior at the stationary state. For the latter experiments, average values of catalytic data were calculated from the last 15 min of each stage. The effluent composition was monitored continuously by sampling online to a quadrupole mass spectrometer (Balzers QMS 421) equipped with a Faraday detector (0–200 amu). Nine masses characteristic of NO (30), NO_2 (30, 46), N_2O (28, 30, 44), $^{14}N_2$ (28), $^{15}N^{14}N$ (29), NH_3 (17, 18), H_2O (17, 18), O_2 (16, 32), and He (4) were followed. The intensities of NH_3 (17), H_2O (18), $^{14}N_2$ (28), $^{14}N^{15}N$ (29), and NO (30) were determined by solving a linear system of equations. The concentrations were derived from intensities by using prior standardization procedures.

RESULTS

Physicochemical Properties of the Catalysts

The chemical analyses and the textural properties are given in Table 1 for the various samples. The unit cell content for the Cu-exchanged catalysts was estimated from the chemical analysis. For the Cu-exchanged zeolites the removed sodium, in the form of Na^+, is compensated mainly by the introduction of Cu^{2+}. The specific surface area and the micropore volume of the heavily loaded Cu(195)/FAU prepared by impregnation are low compared with those of the parent Na-FAU. This is very likely due to pore blocking, since the X-ray diffraction pattern of Cu(195)/FAU is very similar to that of Na-FAU which provides evidence of a very small collapse of the zeolite structure on Cu impregnation.

The diffuse reflectance spectra of the as-stored samples are shown in Fig. 1. All the spectra exhibit the $O \rightarrow Cu^{2+}$ charge transfer transitions occurring at 225 nm. For Cu(x)-FAU ($x \leq 76$) a characteristic band of Cu^{2+} ions in an octahedral environment was observed at 800–850 nm (Figs. 1a–1c). Schoonheydt (20) attributed this band to the copper

TABLE 1

Main Physicochemical Characteristics of the Samples

Sample	Chemical analyses (wt%) Cu	Na	Al	Si	S_{BET} (m^2 g^{-1})	Volume in micropores (cm^3 g^{-1})	Unit cell content
Na-FAU	0	6.79	8.46	23.0	700	0.35	$Na_{49.9}H_{3.1}Al_{53}Si_{139}O_{384}$
Cu(25)-FAU	2.91	5.80	9.76	24.6	680	0.32	$Cu_{7.1}Na_{39.1}H_{2.8}Al_{56}Si_{136}O_{384}$
Cu(37)-FAU	3.84	4.56	8.75	23.2	630	0.32	$Cu_{10.1}Na_{33}H_{0.8}Al_{54}Si_{138}O_{384}$
Cu(56)-FAU	5.72	3.12	8.68	22.1	660	0.34	$Cu_{15.6}Na_{23.5}H_1Al_{56}Si_{136}O_{384}$
Cu(76)-FAU	7.24	1.97	8.09	22.3	670	0.34	$Cu_{20}Na_{15}Al_{53}Si_{139}O_{384}$
Cu(195)/FAU	17.64	6.08	7.68	20.9	300	0.15	—

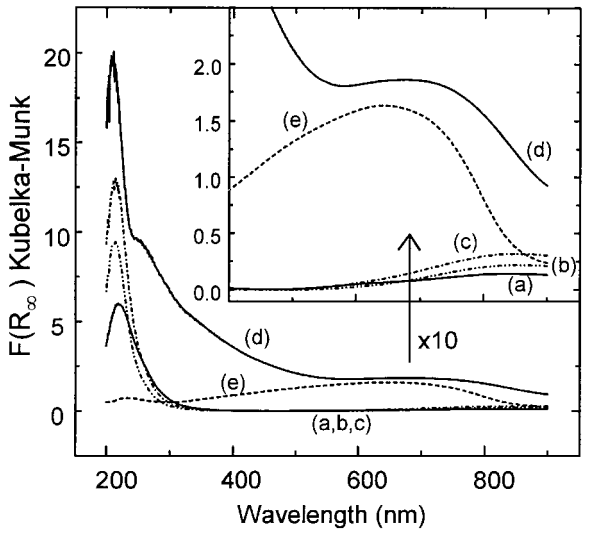

FIG. 1. Diffuse reflectance spectra of the samples as stored: (a) Cu(25)-FAU, (b) Cu(56)-FAU, (c) Cu(76)-FAU, (d) Cu(195)/FAU, (e) 10% CuO/SiO_2.

$^2E_g \rightarrow {}^2T_{2g}$ transition. Cu(195)/FAU behaves differently since the spectrum exhibits a large band at 700–750 nm (Fig. 1d), which can be compared with the band at 600–750 nm observed in 10% CuO/SiO_2 as reference (Fig. 1e); this band is attributed to the *d–d* transition of Cu with octahedral environment in CuO, as proposed in the case of zirconia (21)- and alumina (22)-supported CuO. It should be pointed out that the XRD pattern of Cu(195)/FAU exhibits the (111) line of CuO, and a mean size of 25 nm for the CuO crystallites has been calculated from the line broadening. We have, therefore, two groups of catalysts: those that contain mainly isolated Cu^{2+} species and Cu/FAU with CuO aggregates.

TPR and TPO Experiments

The TPR profiles of the Cu-FAU samples are shown in Fig. 2. For Cu(x)-FAU ($x \leq 76$) two groups of peaks are observed at low temperatures (LT, 450–700 K) and at high temperature (HT, >1000 K). In agreement with previous reports (19, 23–25), the LT and HT peaks can be assigned to the $Cu^{2+} \rightarrow Cu^+$ and $Cu^+ \rightarrow Cu^0$ reduction steps, respectively. Cu(76)-FAU, which was indeed blue at the onset of the TPR, turned white (color of Cu^+) when the TPR was stopped at 750 K and became purple (characteristic of Cu^0 aggregates) after TPR up to 1250 K. The LT profiles are composed of two unresolved peaks at ca. 520 K and 650 K for Cu(x)-FAU ($x \leq 76$), with a small shoulder at 750–800 K for Cu(76)-FAU. Similar TPR profiles in this temperature range were observed by Gentry *et al.* (25) on Cu-FAU; they assigned each peak to the reduction of Cu^{2+} species in different lattice positions of FAU.

The TPR profile of Cu(195)/FAU, which contains mainly CuO, exhibits a large peak at 575 K and a small contribution at 950–1000 K (Fig. 2e). As previously proposed (26, 27), the first peak occurring at 575 K corresponds to the one-step reduction of CuO to Cu^0 aggregates. Considering the attribution of the reduction peaks for Cu(x)-FAU ($x \leq 76$) (see above), we can assume that the HT peak at 990 K of Cu(195)/FAU is due to the $Cu^+ \rightarrow Cu^0$ reduction step of a small fraction of Cu species; the corresponding $Cu^{2+} \rightarrow Cu^+$ step very likely contributes to the first broad H_2 consumption peak at ca. 575 K. The temperatures at the maximum of each peak of TPR profiles are collected in Table 2, as is the total H_2 consumption (H_2/Cu). To determine the quantities of H_2 consumed under each individual contribution, the deconvolution of the broad feature between 400 and 700 K was undertaken graphically by assuming symmetrical profiles (Figs. 2a–2d). Basically, this assumption is not founded by theory, but the results appear satisfactory enough to allow correct estimation of the different contributions. It appears that H_2/Cu is lower than 1 for Cu(x)-FAU ($x \leq 76$). This is due in part to the autoreduction of Cu^{2+} to Cu^+ by activation at ca. 700 K in inert atmosphere (24, 28). The hydrogen consumed under the HT peak (>1000 K) indeed represents $H_2/Cu \approx 0.40$–0.47.

The TPO profiles of Cu(76)-FAU, prereduced by NH_3 at 773 K for 30 min and then evacuated at the same temperature, are shown in Fig. 3. This pretreatment selectively reduces Cu^{2+} to Cu^+ (9, 19) with a color change of the sample from blue to white. NO alone is inefficient in reoxidizing Cu^+ under the present conditions. In contrast O_2, or better

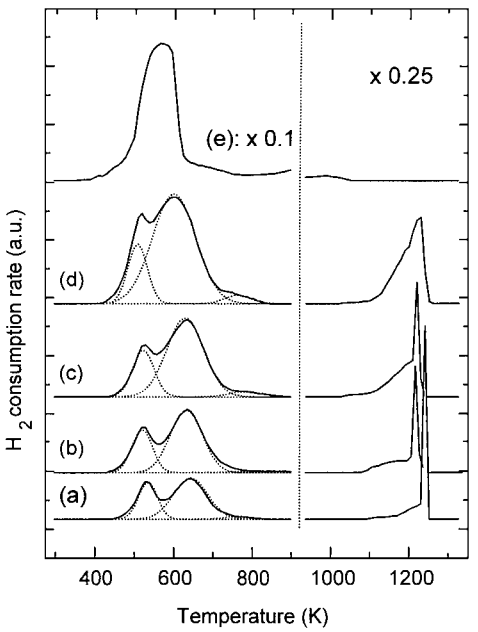

FIG. 2. Temperature-programmed reduction profiles of Cu-FAU catalysts: (a) Cu(25)-FAU, (b) Cu(37)-FAU, (c) Cu(56)-FAU, (d) Cu(76)-FAU, (e) Cu(195)/FAU. $m \approx 50$ mg, gas = H_2/Ar (3/97, v/v), ramp = 10 K min^{-1}, flow rate = 18.6 cm^3 min^{-1}.

TABLE 2

Quantitative Analysis of the TPR Profiles of Cu-FAU (from Fig. 2)

Sample	T_M (K) and % H_2 consumption				H_2/Cu (mol/mol)
	$Cu^{2+} \rightarrow Cu^+$				
	First peak	Second peak	$Cu^+ \rightarrow Cu^0$	$CuO \rightarrow Cu^0$	
Cu(25)-FAU	535 (11%)	645 (31%)	1270 (52%)	—	0.76
Cu(37)-FAU	520 (13%)	635 (34%)	1255 (53%)	—	0.82
Cu(56)-FAU	515 (11%)	630 (37%)	1250 (56%)	—	0.80
Cu(76)-FAU	495 (9%)	600 (38%)	1225 (53%)	—	0.84
Cu(195)/FAU	≈575 (10%)	—	990 (10%)	575 (80%)	1.1

a mixture of O_2 and NO, can do it. With O_2 alone, the faster oxidation rate occurred at 625 K, with concurrent H_2O evolution. With the NO + O_2 mixture, there were two NO and O_2 consumptions, one at ca. 600 K and a shoulder at ca. 450–500 K. The concurrent formation of H_2O and N_2 was also detected in both peaks. The same behavior was observed for TPO with O_2 or O_2 + NO of prereduced Cu(56)-FAU. In both cases the sample turned from white to blue. In contrast, the shoulder at ca. 450–500 K was hardly visible in the TPO of Cu(37)-FAU by NO + O_2 and could not be identified for Cu(25)-FAU. The data derived from these experiments, i.e., the temperatures for the faster oxidation rates (T_M), NO and O_2 consumption, and N_2 and H_2O formation, are listed in Table 3. Average values for the NO/O_2 consumption ratio of 3 and 1 were found for the first (450–500 K) and second (600 K) peaks, respectively. That N_2 formation was in good agreement with the NO consumption in the case of Cu(76)-FAU, but less for Cu(56)-FAU, may be due to sensitivity problems. The water evolution is also lower than expected; this can be explained by a rehydroxylation of the zeolite by H_2O formed in the course of the TPO; the pretreatment in NH_3 at 773 K and the outgassing with He at the same temperature most probably initiate the facile annealing of the hydrogen-bonded silanols.

TPD and FTIR Spectroscopy of Adsorbed NH_3 and NO

The TPD profiles of NH_3 after adsorption at room temperature on Na-FAU, Cu(x)-FAU ($x \leq 76$), and Cu(195)/FAU are shown in Fig. 4. One should first point out that the samples remained blue at the end of the TPD (Cu^{2+} was hardly reduced). The TPD profile on Na-FAU (Fig. 4a) is composed of a broad peak with two maxima at 380 and 420 K, whereas an additional peak appears above 500 K for the Cu(x)-FAU samples. This is particularly clear for Cu(76)-FAU with the NH_3 desorption at ca. 600 K (Fig. 4d). We can then attribute this HT peak to NH_3 desorbing from Cu^{2+} ions. Both Cu^{2+} and Na-FAU sites contribute to the large amount of NH_3 that desorbs between 300 and 500 K. The TPD profile of NH_3 from Cu(195)/FAU (Fig. 4e) is very similar to that recorded with Na-FAU, no desorption of NH_3 at high temperature, providing evidence that CuO species adsorb NH_3 very weakly.

Additional information was provided by FTIR spectra recorded at room temperature, after evacuation at

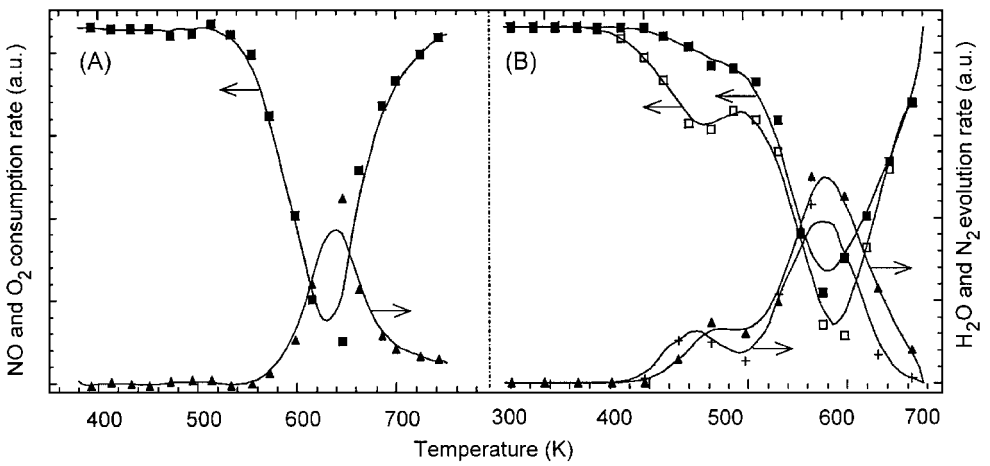

FIG. 3. Temperature-programmed oxidation of Cu(76)-FAU with different oxidants: (A) TPO by O_2 (2000 ppm in helium), (B) TPO by O_2 + NO (2000 + 2000 ppm in helium); (■) O_2, (▲) H_2O, (□) NO, (+) N_2. $m = 50$ mg, ramp = 5 K min^{-1}, flow = 50 cm^3 min^{-1}.

TABLE 3

Quantitative Analysis of the TPO Profiles of Cu(56)-FAU and Cu(76)-FAU Prereduced by NH_3/He (10/90) at 773 K

			Consumption (μmol g^{-1})				Formation (μmol g^{-1})				
	T_M (K)		NO		O_2		N_2		H_2O		
Sample	First peak	Second peak	First peak	Second peak	First peak	Second peak	First peak	Second peak	First peak	Second peak	$(2O_2 + NO)/Cu^a$
Cu(37)-FAU[a]	nd	570	nd	60	nd	70	nd	25	nd	20	0.38
Cu(56)-FAU[a]	500	580	26	90	9	90	7	20	16	60	0.36
Cu(76)-FAU[a]	505	580	38	150	12	130	15	70	17	95	0.43
Cu(76)-FAU[b]	—	640	—	—	—	260	—	—	—	250	0.46

[a] TPO by $O_2 + NO$.
[b] TPO by O_2.

increasing temperatures of the sample contacted with NH_3 at room temperature. After outgassing Na-FAU at 350 K, five bands appear at 3398, 3370, 3319, 3269, and 1641 cm^{-1}, and a very broad feature centered around 1550 cm^{-1} (Fig. 5A). In agreement with the band assignment proposed by Datka *et al.* (29), for NH_3 adsorbed on Na-MOR, we suggest that the band at 3370 cm^{-1} is due to NH_3 bonded on Lewis acid sites, the bands at 3398, 3318, and 1641 cm^{-1} are due to NH_3 bonded on Na^+, and the bands at 3269 and 1550 cm^{-1} are due to NH_3 bonded on Brønsted sites of extraframework AlOH and framework AlOH located in the supercages, as revealed by the IR spectrum of NH_3 free Na-FAU (Fig. 5B). We have not observed the band at low frequency of framework AlOH located in the sodalite cages which are likely exchanged by Na. The adsorbed NH_3 species are decomposed above 470 K (Fig. 5A), in agreement with previous work (30).

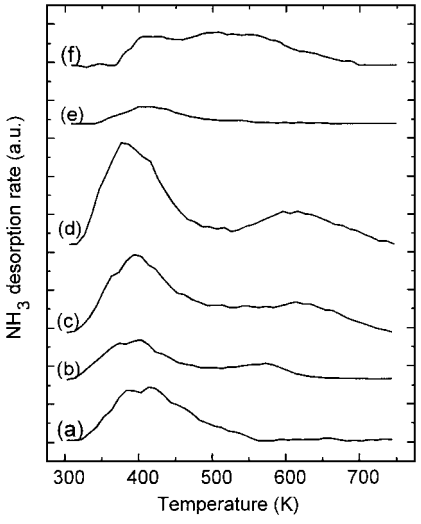

FIG. 4. Temperature-programmed desorption profiles of NH_3 from Na-FAU and Cu-FAU catalysts: (a) Na-FAU, (b) Cu(25)-FAU, (c) Cu(56)-FAU, (d) Cu(76)-FAU, and (e) Cu(195)/FAU after He treatment at 773 K and NH_3 adsorption at room temperature, desorption in He flow; (f) Cu(76)-FAU after NH_3 treatment at 773 K, desorption in He at 773 K followed by NH_3 adsorption at room temperature. $m \approx 20$ mg, ramp = 5 K min^{-1}, flow = 50 cm^3 min^{-1}.

After NH_3 adsorption on the Cu(76)-FAU sample and evacuation at 350 K, the FTIR spectrum shows additional bands at 3393, 3346, 3300, 3216, 3177, 1613, and 1280 cm^{-1} which appear with some of the existing bands on the Cu-free Na-FAU (Fig. 6). In a FTIR study of NH_3 adsorbed on Cu-FAU zeolites, Howard and Nicol (31) and Flentge *et al.* (32) attributed these bands to the formation of $[Cu(NH_3)_n]^{2+}$ complexes within the zeolite cages. On heating, the bands due to NH_3 adsorbed on the support disappear first below 470 K, whereas the bands of $[Cu(NH_3)_n]^{2+}$ complexes still remain at 520 K; above 570 K the complexes are fully decomposed. On NH_3 adsorption, the FTIR spectra of Cu(25)-FAU and Cu(56)-FAU exhibit the same bands, although less intense, as in the Cu(76)-FAU spectrum, whereas the Cu(195)/FAU spectrum is very similar to that of Na-FAU.

The total amounts of NH_3 that desorbed from the samples are as follows: Na-FAU, 1360 μmol g^{-1}; Cu(25)-FAU, 1500 μmol g^{-1}; Cu(56)-FAU, 2860 μmol g^{-1}; Cu(76)-FAU, 3610 μmol g^{-1}; Cu(195)/FAU, 490 μmol g^{-1}. The amount of NH_3 that desorbed under the peak centered at ca. 620 K from Cu(76)-FAU (Fig. 4d) represents 1200 μmol g^{-1}. This value is very close to the 1140 μmol g^{-1} of Cu contained in this sample. From TPD and FTIR spectroscopy we can reasonably conclude that the HT peak of NH_3 desorption from Cu(x)-FAU corresponds to the release of the last NH_3 ligand from $[Cu(NH_3)_n]^{2+}$ complexes. The broad peak ($300 < T < 500$ K, Figs. 4c, 4d) of NH_3 desorption from Cu(56)-FAU and Cu(76)-FAU represents 2050 and 2400 μmol g^{-1}, respectively. For Na-FAU, an average of 0.46 NH_3 per Na was found. Therefore, 1230 and 2020 μmol g^{-1} approximately can be accounted for by NH_3 desorption from $[Cu(NH_3)_n]^{2+}$ of Cu(56)-FAU ($Cu^{2+} = 900$ μmol g^{-1}) and of Cu(76)-FAU ($Cu^{2+} = 1140$ μmol g^{-1}). From these observations, one can conclude that an average of two NH_3 molecules per Cu site are released in the LT TPD peak.

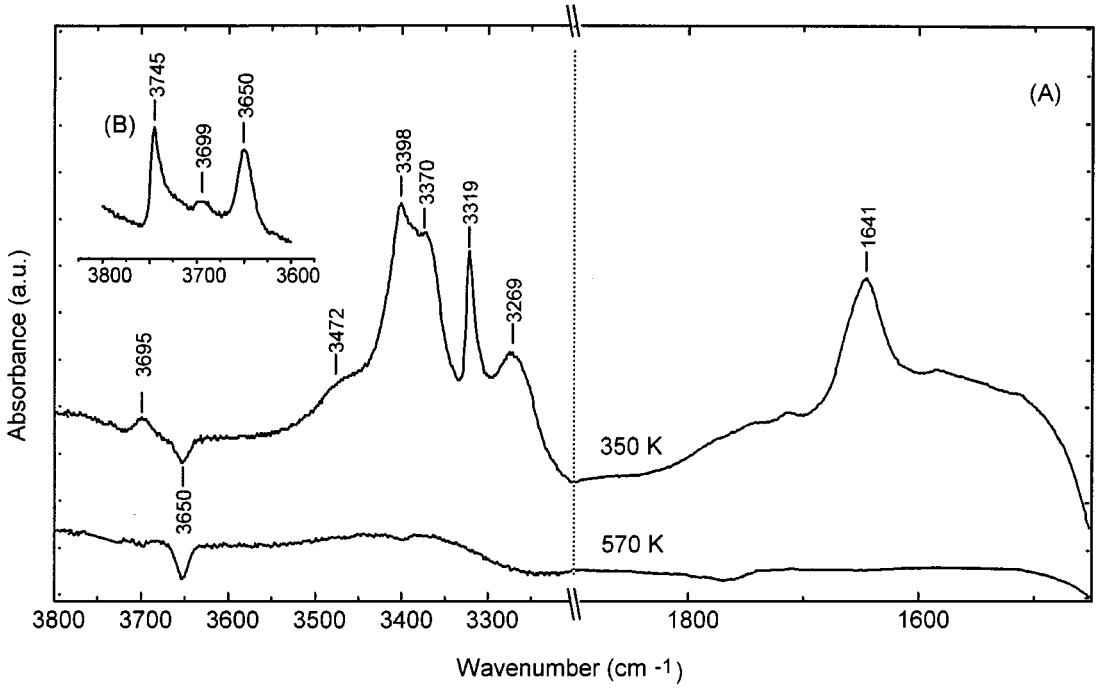

FIG. 5. (A) Infrared spectra of Na-FAU contacted with NH_3 at room temperature then evacuated at increasing temperatures. (B) IR spectrum of NH_3-free Na-FAU; the spectra were recorded after cooling at room temperature.

To sum up, the average number n of NH_3 ligands in the $[Cu(NH_3)_n]^{2+}$ complexes formed by NH_3 adsorption at room temperature and subsequent evacuation is 3. Huang and Vansant (33) found by gravimetry a desorption of 3.3 NH_3 per Cu^{2+} species for a series of Cu-FAU samples, with different Cu loadings, and concluded that the complex was $[Cu(NH_3)_4]^{2+}$ by reference to ESR experiments carried out at 77 K (34). Our results indicate that only three NH_3

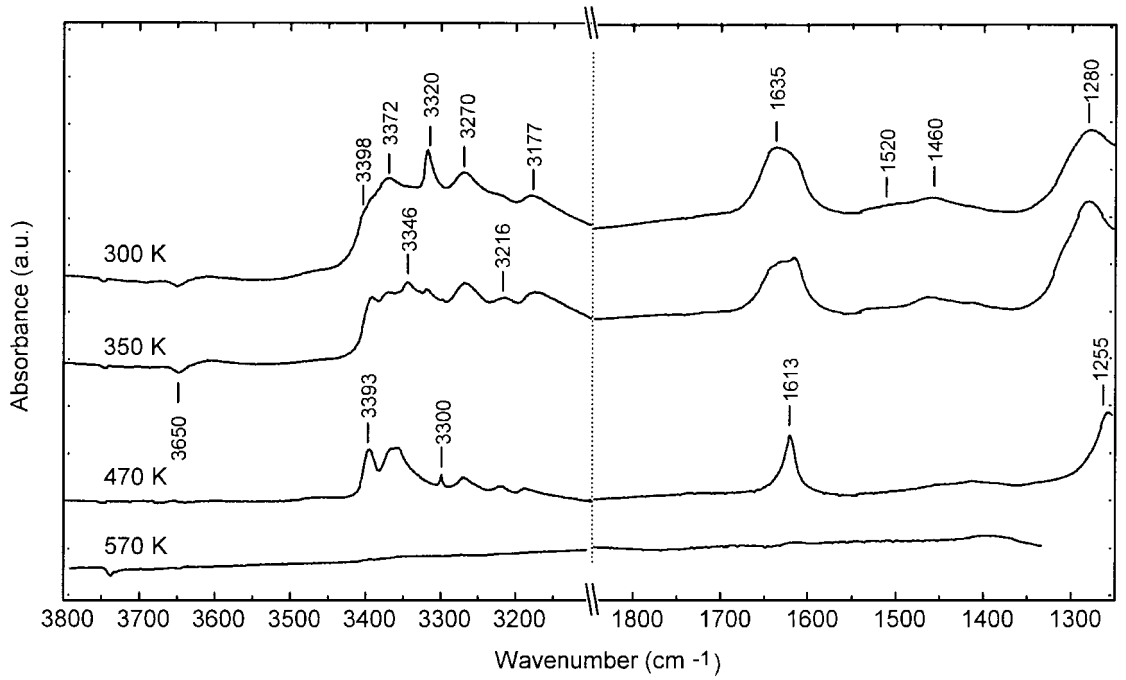

FIG. 6. Infrared spectra of Cu(76)-FAU contacted with NH_3 at room temperature then evacuated at increasing temperatures; the spectra were recorded after cooling at room temperature.

ligands are bound to Cu^{2+} ions in the dehydrated Cu-FAU. Nevertheless, it may be possible that some isolated Cu^{2+} ions remain inaccessible to NH_3 or have less coordinated NH_3 ligands. Moreover, a partial reduction of Cu^{2+} to Cu^+ could also be considered.

For Cu(76)-FAU sample (Fig. 4f), prereduced with NH_3 at 773 K ($Cu^{2+} \rightarrow Cu^+$), the TPD profile of NH_3 exhibits a broad peak from 350 to 600 K. This peak represents ca 1500 μmol g^{-1} NH_3 desorbing from Cu sites, i.e., 1.4 NH_3/Cu^+. The complex that might be formed would be a $[Cu(NH_3)_2]^+$ complex, as already proposed (33).

The adsorption/desorption of NO on the same samples was studied by TPD and FTIR. It appeared that the strength of NO adsorption on Cu-FAU was weak, since NO was released by flushing with He at room temperature. This emphasizes the unusual behavior of Cu-FAU compared with Cu-MFI (16) and Cu-MOR (35, 36) for which NO desorption was observed until 873 and 673 K, respectively.

Selective Catalytic Reduction of NO by NH_3

It was first checked that no NO conversion occurred on the Cu free Na-FAU sample. The possible occurrence of intraparticle mass transfer limitations was furthermore checked on Cu(76)-FAU. After grinding and sieving, in the ranges 63–125 and 250–400 μm, two aliquots were tested for the SCR of NO by NH_3 in a TPSR protocol. The plots of NO conversion to N_2 were quasi-superimposed for the two aliquots which provides evidence that the intraparticle mass transfer is fast enough and will not screen the chemical processes.

The conversion profiles of NO and NH_3, as well as the selectivity in N_2 and N_2O, for the SCR of NO by NH_3 on Cu(76)-FAU in TPSR protocol, and the NO conversion at the stationary state, are presented in Fig. 7A. In TPSR the NO conversion profile exhibits two peaks at 420 and 520 K, before reaching 100% above 620 K. The first peak of NO conversion was observed by several authors using a similar protocol of catalytic tests (8, 13, 14). However, at the stationary state, by decreasing the temperature from 700 to 300 K in steps of 25 K, the wave of NO conversion around 400 K disappeared (Fig. 7A). In this case, a gap always exists between the conversions of NH_3 and NO, except at full NO conversion. One should point out that the NO conversions found under steady-state conditions were very close to that found in the TPSR experiment above 450 K. These experiments show that the first wave of NO conversion at 420 K is a transient phenomenon due to the TPSR protocol. *In situ* UV–visible spectroscopy has shown that (i) Cu^{2+} is transformed into Cu^+ at 450 K after the first wave of NO conversion, and (ii) in the reduction of NO by NH_3 in the absence of O_2, Cu^+ formed at 450 K is not regenerated below 773 K, and the reaction then stops.

Figure 8 shows the conversion of NO and the selectivity to N_2O found at the stationary state on Cu(x)-FAU ($x \leq 76$). It is clear (i) that the activity decreases with decreasing Cu content, and the wave of NO conversion at ca. 500 K tends to disappear, and (ii) that the selectivity to N_2O decreases at both low and high temperatures at low Cu content. The NO conversions on Cu(80)-MFI and Cu(69)-MOR are also plotted in the same figure (Fig. 8A).

Figure 7B presents the SCR on Cu(195)/FAU ($x \leq 76$). The conversion profile of NO is very different from those observed on Cu(x)-FAU. There is a bell-shaped profile as a function of temperature for both NO conversion and N_2O selectivity. NO conversion goes through a maximum of 70% at 570 K, then decreases to 25% at 770 K, and the conversion in NH_3 is total at this temperature. Similar SCR profiles were observed with ZrO_2-, TiO_2-, and Al_2O_3-supported CuO catalysts (22, 37).

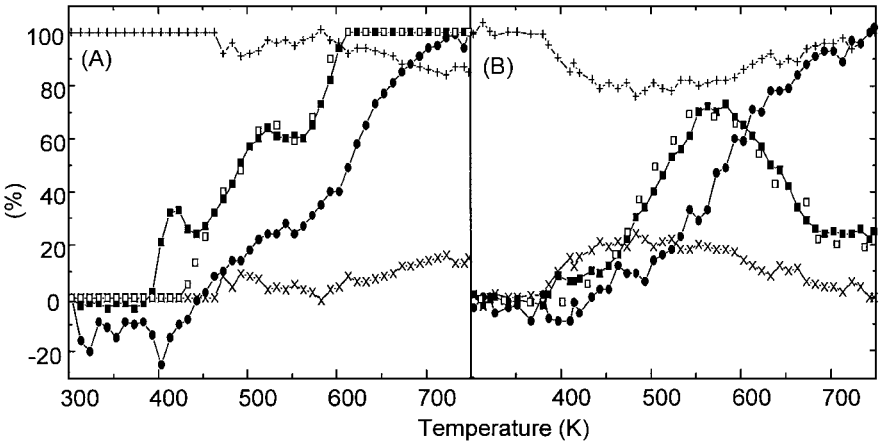

FIG. 7. SCR of NO by NH_3 over Cu-FAU catalysts as a function of temperature: (A) Cu(76)-FAU, (B) Cu(195)/FAU. (■) NO and (●) NH_3 conversion. (+) N_2 and (×) N_2O selectivity obtained in the TPSR protocol (ramp = 5 K min^{-1}, VVH = 250,000 h^{-1}). (□) NO conversion obtained in steady-state experiments by decreasing the temperature from 773 to 300 K in steps of 25 K (VVH = 250,000 h^{-1}).

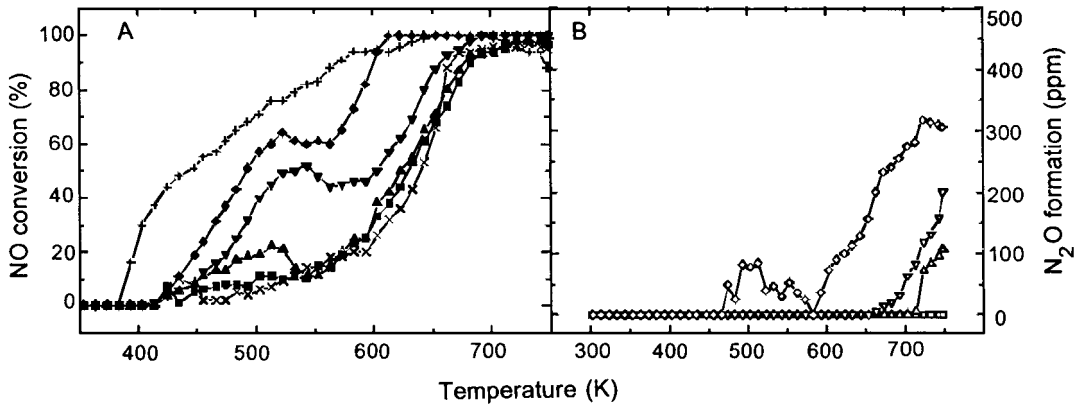

FIG. 8. SCR of NO by NH_3 in steady-state experiments on Cu(76)-FAU (◆, ◇), Cu(56)-FAU (▼, ▽), Cu(37)-FAU (▲, △), Cu(25)-FAU (■, □), Cu(80)-MFI (×), and Cu(69)-MOR (+). (A) NO conversion, (B) N_2O selectivity.

DISCUSSION

Nature, Siting, and Redox Properties of Cu Species in Cu-FAU Catalysts

UV–vis spectroscopy and XRD and TPR experiments have shown that copper is in the form of CuO in Cu(195)/FAU and of Cu^{n+} species in Cu(x)-FAU ($x \leq 76$).

TPR experiments provide evidence for the reduction of Cu^{2+} occupying different locations in Cu(x)-FAU (Fig. 2). By using similar TPR conditions, Gentry *et al.* (25) observed two reduction peaks of Cu^{2+} to Cu^{+} in Cu(68)-FAU at ca. 523 and 620 K. The former was assigned to Cu^{2+} located in the supercages and the latter to Cu^{2+} in sodalite cavities. Easier reducibility of Ni^{2+} in supercages (sites II) compared with those in sodalite cavities (sites I′ and II′) was also reported for variously exchanged Ni-FAU (38). From the deconvolution of the LT peak in TPR profiles of Cu(x)-FAU (Fig. 2 and Table 2), the surface area ratio of the first and second peaks decreases from 0.35 for Cu(25)-FAU to 0.24 for Cu(76)-FAU. From XRD diffraction patterns of dehydrated Cu(80)-FAU Maxwell and de Boer (39) suggested the following distribution of Cu^{2+} ions within the zeolite framework: 23% in the supercage (site II), 66% in the sodalite cavity (sites I′ and II′), and 11% in the hexagonal prism (site I). From these observations we can attribute the first component (at 495–535 K) in the LT peak of Cu(x)-FAU to reduction of Cu^{2+} species located in the supercages, and the second component at 600–645 K to Cu^{2+} species occupying sodalite cavities. The small shoulder which can be identified at 750–800 K in the TPR profile of Cu(76)-FAU (Fig. 2d) can be assigned to the reduction of Cu^{2+} in hexagonal prisms; the corresponding H_2 consumption was taken into account in the second component of the deconvoluted LT peak. The decrease in the surface area ratio of the first and second components from Cu(25)- to Cu(76)-FAU emphasizes the higher selectivity of Cu^{2+} to occupy the supercages with respect to sodalite cavities at low Cu exchange, in agreement with previous reports (20, 40, 41). An estimation of the distribution of Cu^{2+} among locations in supercages and sodalite cavities in dehydrated Cu(x)-FAU is given in Table 4.

On treatment of Cu(x)-FAU at 773 K in NH_3/He, Cu^{2+} is transformed into Cu^{+} and the subsequent outflowing in He at the same temperature leads to dehydrated and NH_3-free Cu(x)-FAU. This is an important point since H_2O could promote the oxidation of Cu^{+} by O_2 at low temperature as shown in Cu-MFI (42). After cooling to room temperature, the oxidability of these Cu^{+} species depends on both the sample and the oxidant mixture. For all the samples, Cu^{+} is oxidized in one step to Cu^{2+} with O_2 alone which shows an undifferentiated process whatever location of these Cu^{+} species. In contrast, the TPO profiles carried out with $O_2 + NO$ exhibit two peaks with Cu(76)-, Cu(56)-, and Cu(37)-FAU, but only one with Cu(25)-FAU. This behavior can be compared with the two contributions observed in the LT peaks on the TPR profile. On that account, we could assign the LT peak in the TPO of Cu(37)-, Cu(56)-, and Cu(76)-FAU with $O_2 + NO$ to the oxidation of Cu^{+} located in the supercages. The absence of the LT peak in the TPO of Cu(25)-FAU could be explained by the higher selectivity of Cu^{+} compared with Na^{+} for sodalite

TABLE 4

Proposition for the Distribution of Cu^{2+} per Unit Cell in Dehydrated Cu(x)-FAU ($x \leq 76$)

Sample	Total Cu atoms (per unit cell)	Location		
		Supercage	Sodalite[a]	Unlocalized
Cu(25)-FAU	7.1	1.6	3.9	1.6
Cu(37)-FAU	10.1	1.8	4.7	2.2
Cu(56)-FAU	15.6	2.5	8.4	4.7
Cu(76)-FAU	20.0	3.2	13.6	3.2

[a] including hexagonal prism.

sites, the unique speciation of some Cu^+ entities that exist only with Cu(37)-, Cu(56)-, and Cu(76)-FAU for promoting oxidation of Cu^+ to Cu^{2+} in supercages at low temperature, and/or sensitivity problems in mass spectrometry. Anyway, the key point is that a synergistic effect between NO and O_2 for the oxidation of Cu^+ to Cu^{2+} exists whatever the catalyst, as shown by the lower temperature of oxidation (Table 3). Taking into account the amounts of O_2 and NO consumed in the LT ($NO/O_2 \approx 3$) and the HT ($NO/O_2 \approx 1$) peaks of Cu(56)- and Cu(76)-FAU, we can propose two formal oxidation reactions of Cu^+ species:

(1) at 500 K, oxidation of Cu^+ located in the supercages,

$$10Cu^+ + 3NO + O_2 + 10H^+ \rightarrow 10Cu^{2+} + 5H_2O + \tfrac{3}{2}N_2; \quad [2]$$

(2) at 580 K, oxidation of Cu^+ located in sodalite cavities,

$$6Cu^+ + NO + O_2 + 6H^+ \rightarrow 6Cu^{2+} + 3H_2O + \tfrac{1}{2}N_2; \quad [3]$$

The oxidation of Cu^+ to Cu^{2+} by O_2 alone at 640 K corresponds to the reaction

$$4Cu^+ + O_2 + 4H^+ \rightarrow 4Cu^{2+} + 2H_2O \quad [4]$$

and does not compete with the former reaction (Eq. [3]) at temperatures below ca. 650 K.

The stoichiometries of Eqs. [2] and [3] should be considered only indicative and not definite values. This point addresses the exact nature of the superactive intermediate formed between NO and O_2 in the course of the TPO. A wide variety of nitrogen oxides exist and characteristics bands of NO_2, N_2O_4, and N_2O_5 have been identified by Szanyi and Paffett (43) by contacting NO and O_2 on Cu-MFI at room temperature. Adsorbed N_2O_3 has also been proposed as a reactive intermediate in the SCR of NO on Cu-MFI (44). With regard to the different stoichiometries of Eqs. [2] and [3] we can just postulate that the intermediates are different for the oxidation of Cu^+ located in the supercages or the sodalite cavities.

SCR of NO by NH_3 on Cu-FAU

The two classes of catalysts, i.e., Cu(195)/FAU and Cu(x)-FAU ($x \leq 76$), are different in their behavior. The conversion of NO steadily increases with temperature on the latter samples (Fig. 7A), but goes through a maximum of 70% conversion at ca. 570 K on Cu(195)/FAU (Fig. 7B). This is due to the oxidation of NH_3 by O_2, a reaction that competes with the SCR and dominates at high temperature on the CuO aggregates of Cu(195)/FAU sample (45). The oxidation of NH_3 on Cu(195)/FAU yields N_2 and N_2O below 600 K ($N_2/N_2O \approx 5.8$), but the NO formation sharply increases above 600 K (45). The same bell-shaped profile centered at ca. 560 K was reported by Centi *et al.* (22) for the SCR of NO by NH_3 on CuO/Al_2O_3. A significant selectivity to N_2O (up to 20% at 520 K) is observed on Cu(195)/FAU (Fig. 7B). Centi *et al.* (22) reported N_2O selectivities usually lower than 8% for the SCR on variously loaded CuO/Al_2O_3, and underlined that N_2O originated from the formation of ammonium nitrate as intermediate.

With respect to the Cu(x)-FAU samples, the first comment deals with the different conversion profiles of NO when the SCR is carried out either at the stationary state or in TPSR protocol. In TPSR a first peak of NO conversion appears at ca. 420 K, a temperature that merely corresponds to the first desorption of NH_3 from Cu(x)-FAU in TPD experiments (Fig. 4). A similar volcano-shaped NO conversion profile centered at ca. 400 K was previously reported for the reduction of NO by NH_3 on Cu-FAU in the absence of O_2 (12, 13). This was due to the transformation of Cu^{2+} into Cu^+ by $NO + NH_3$ with N_2 release, Cu^+ being not easily regenerated. UV–vis spectroscopy has indeed shown that Cu^{2+} is transformed into Cu^+ after the first peak at 450 K in TPSR. The mechanism for the NO conversion occurring at ca. 420 K can then be expressed as

$$[Cu(NH_3)_3]^{2+} \rightarrow [Cu(NH_3)_2]^{2+} + NH_3, \quad [5]$$

$$[Cu(NH_3)_2]^{2+} + NO \rightarrow [Cu(NH_3)_2NO]^{2+}, \quad [6]$$

$$[Cu(NH_3)_2NO]^{2+} \rightarrow [Cu(NH_3)H]^{2+} + N_2 + H_2O, \quad [7]$$

$$[Cu(NH_3)H]^{2+} \rightarrow [Cu(NH_3)]^{+} + H^{+}. \quad [8]$$

Catalytic activity requires the upkeep of the $Cu^{2+} \leftrightarrow Cu^+$ cycle, since Cu^{2+} is the most active species. Under our operating conditions, Cu^+ was not regenerated at 450 K, even in the presence of O_2, as UV–vis spectroscopy showed.

In the stationary state, two waves of NO conversion at 450–500 K and above 600 K exist on Cu(76)- and Cu(56)-FAU, and the former tends to disappear on Cu(37)- and Cu(25)-FAU (Fig. 8). We showed above that at 450 K copper is in the form of Cu^+ and that the onset of catalytic activity above 450 K comes from the upkeep of the redox cycle $Cu^{2+} \leftrightarrow Cu^+$. It corresponds with the temperature of oxidation of Cu^+ located in supercages with maximum at 470–500 K in the TPO of Cu(76)- and Cu(56)-FAU by $NO + O_2$ (Fig. 3). It must be highlighted that this first peak is very small for Cu(37)-FAU and was not identified for Cu(25)-FAU, a sample that exhibits a rather low SCR activity in the range 450–550 K as well (Fig. 8).

According to this we can suggest that the active sites for NO reduction in the range 450–500 K are Cu species located in the supercages. The upkeep of the catalytic cycle is achieved by $NH_3 + NO$ for the step $Cu^{2+} \rightarrow Cu^+$ and by $NO + O_2$ for the step $Cu^+ \rightarrow Cu^{2+}$. From the NO/O_2 consumption ratio determined in TPO experiments, the following set of reactions can be established for the catalytic cycle

in the range 450–500 K on Cu species in supercages:

$$3NO + O_2 + 10[Cu(NH_3)]^+ + 10H^+ \rightarrow 10[Cu(NH_3)]^{2+} + 5H_2O + \tfrac{3}{2}N_2 \quad [9]$$

$$10[Cu(NH_3)]^{2+} + 10NH_3 + 10NO \rightarrow 10[Cu(NH_3)_2NO]^{2+} \quad [10]$$

$$10[Cu(NH_3)_2NO]^{2+} \rightarrow 10[Cu(NH_3)]^+ + 10H^+ + 10N_2 + 10H_2O \quad [11]$$

$$10NH_3 + 13NO + O_2 \rightarrow 15H_2O + \tfrac{23}{2}N_2 \quad [12]$$

One NH_3 ligand is maintained on Cu sites since TPD experiments have shown that the last desorption occurred above 550 K. The NH_3/NO stoichiometry in Eq. [12] is different from that claimed on V_2O_5/TiO_2 (Eq. [1]), and sustains on a fundamental chemistry basis recent practice in industrial processes (17). To confirm that N_2 formation in the SCR process originates from two different reactions (Eqs. [9] and [11]), an SCR experiment was carried out with 2000 ppm $^{15}NH_3$, 2000 ppm ^{14}NO, and 3% O_2 at 520 K and full conversion (VVH $\approx$ 80,000 h^{-1}) (Fig. 9). On switching from $^{14}NH_3$ to $^{15}NH_3$ the formation of $^{14}N_2$ (16%) and $^{15}N^{14}N$ (84%) was observed. Moreover, the $^{14}N_2/^{15}N^{14}N$ ratio of 0.19 is in good agreement with the value expected from Eqs. [9] and [11], i.e., 0.15.

All the Cu sites of Cu(x)-FAU ($x \leq 76$), located in both the supercages and sodalite cavities, become active for the SCR of NO at high temperature (>600 K, Fig. 8). In the upkeep of the $Cu^{2+} \leftrightarrow Cu^+$ cycle, the oxidation of Cu^+ to Cu^{2+} by both O_2 and $NO + O_2$ could compete in the high-temperature region (Fig. 3). SCR experiments at 600 K with $^{15}NH_3$ can differentiate the occurrence of these two oxidation steps (see above). On switching from $^{14}NH_3$ to $^{15}NH_3$, the formation of $^{14}N_2$ (8%) and $^{15}N^{14}N$ (92%) demonstrates that the reoxidation of Cu^+ derived mainly from $NO + O_2$. According to the consumption ratio $NO/O_2 \approx 1$ found for the HT peak in TPO experiments (Fig. 3, Table 3), the following set of reactions can be expressed for the catalytic cycle above 600 K:

$$NO + O_2 + 6Cu^+ + 6H^+ \rightarrow Cu^{2+} + 3H_2O + \tfrac{1}{2}N_2 \quad [13]$$

$$6Cu^{2+} + 6NH_3 + 6NO \rightarrow 6[Cu(NH_3)NO]^{2+} \quad [14]$$

$$6[Cu(NH_3)NO]^{2+} \rightarrow 6Cu^+ + 6H^+ + 6N_2 + 6H_2O \quad [15]$$

$$6NH_3 + 7NO + O_2 \rightarrow 9H_2O + \tfrac{1}{2}N_2 \quad [16]$$

There is no more NH_3 ligand permanently bonded to Cu sites at this temperature.

We have shown that an original mechanism operates for the SCR on Cu(x)-FAU ($x \leq 76$). In particular, we have been able to prove the existence of some Cu species in supercages exhibiting high activity at low temperature. The comparative behavior of the various Cu(x)-FAU was examined in more detail with the aim of revealing some aspect of these species. Figure 10 shows the TOF (h^{-1}) determined at 500 K of the SCR on Cu(x)-zeolites. The TOF was calculated by dividing the SCR rate (mol g^{-1} h^{-1}) by the Cu concentration (mol g^{-1}). Rates in the stationary state (Fig. 8) were used for these calculations. When the TOF on Cu(x)-FAU is determined with respect to all the Cu species, the specific reactivity of Cu ions in Cu-FAU is much lower than

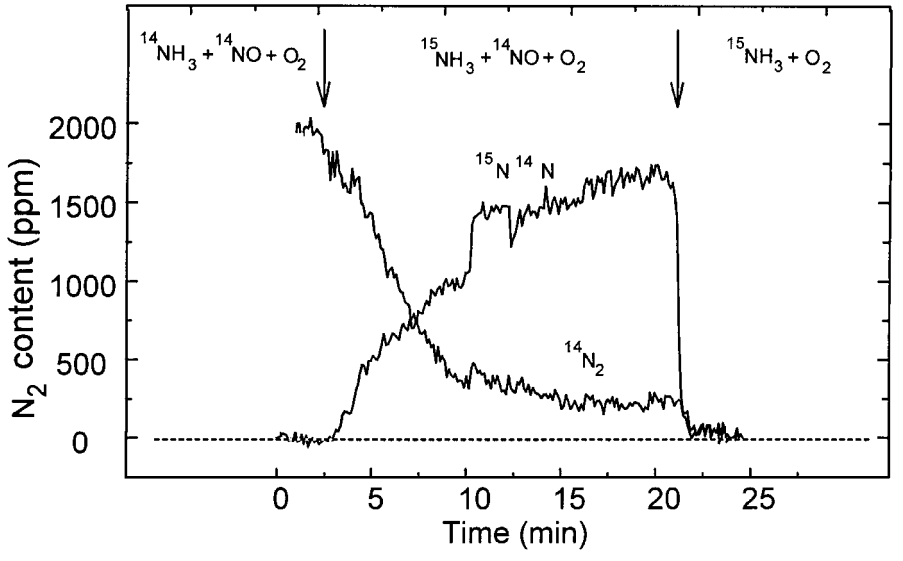

FIG. 9. $^{14}N_2$ and $^{14}N^{15}N$ formation in the SCR of ^{14}NO by $^{15}NH_3$ at 520 K on Cu(76)-FAU (VVH = 80,000 h^{-1}); the conversion of NO is close to 100%.

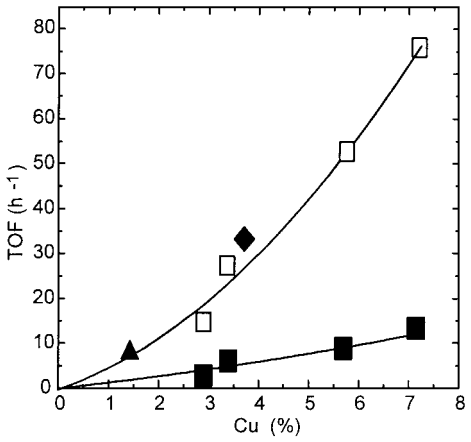

FIG. 10. TOF determined at 500 K in the SCR of NO by NH_3 on Cu-exchanged zeolites: (■) based on the overall concentration of copper in Cu(x)-FAU, (□) based on the concentration of copper located in supercages of Cu(x)-FAU, (▲) Cu(80)-MFI, and (◆) Cu(74)-MOR.

in Cu-MOR or Cu-MFI. However, we concluded above that Cu located in the supercages is the active species at 500 K in Cu(x)-FAU. So, the TOF was calculated again with respect to these species alone (Fig. 10). The amount of these species, taken from Table 4, was derived from TPR experiments in the absence of NH_3, and should be taken cautiously. It is likely underestimated since NH_3 can induce some Cu species to move from sodalite cavities to supercages. The new values of TOF ($TOF_{sup.}$) as determined should only be considered as a tendency. The $TOF_{sup.}$ of Cu(x)-FAU falls on the same plot as TOF of Cu(80)-MFI and Cu(69)-MOR, indicating that the active Cu species in these catalysts are not very different in nature.

A much more interesting behavior is the sixfold increase of $TOF_{sup.}$ with Cu content from 2.9 to 7.2 wt% (Fig. 10). Komatsu *et al.* (9) reported a fourfold increase in the specific activity at 573 K when the Cu content in Cu-MOR and Cu-MFI increased from 2 to 5×10^{-4} mol g^{-1}. They concluded that $[CuOCu]^{2+}$ dimer species are the active sites. Similar species were claimed to govern the decomposition of NO on Cu-MFI (46). It is obvious that the proportion of such species, or next-nearest-neighbor (NNN) Cu ions, should increase with increasing Cu content if Cu ions are located at random at the cation sites. An equilibrium moreover may exist between dimers and NNN Cu species depending on the O_2 partial pressure.

The occurrence of $[CuOCu]^{2+}$ species in the supercages was never observed, and a unique possibility would be two Cu^{2+} ions located in sites II and III. Cu in site II was identified from either TPR or TPO experiments. Cu ions at site III were identified only by XRD experiments on hydrated Cu-Na-FAU (40): Cu^{2+} ion is bonded to two framework oxygens and four H_2O ligands to form an octahedral complex. With increasing temperature, the octahedral complex loses H_2O and Cu moves to site II. It is therefore possible that a complex composed of a Cu bonded to two framework oxygens, three ammonias, and an extra-framework oxygen bridging with a second Cu in site II exists at room temperature (Fig. 11). At 500 K, only one NH_3 should remain,

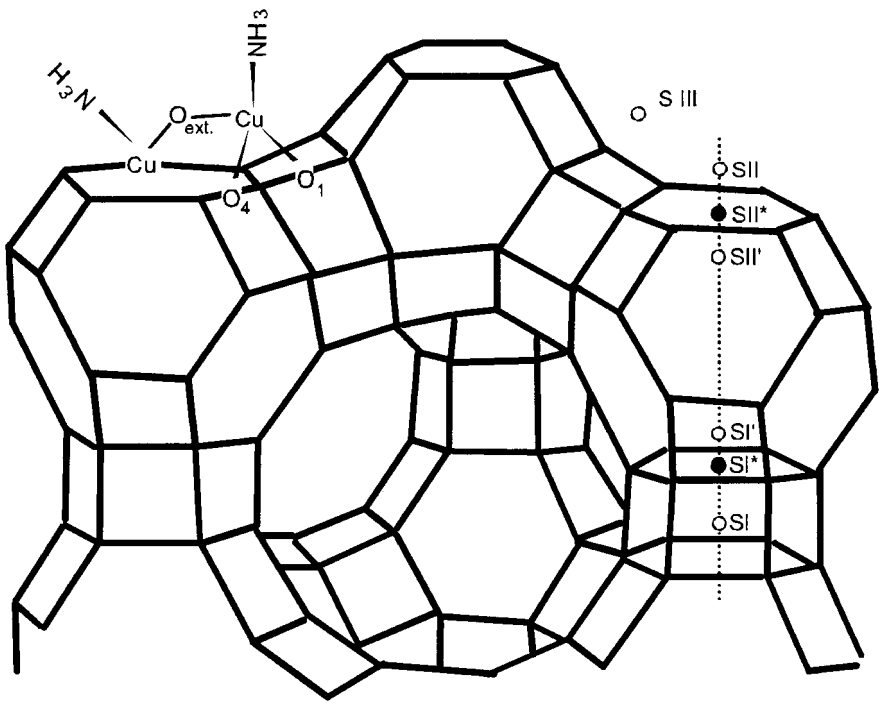

FIG. 11. View of the faujasite structure with the various cationic sites and the proposed location of $[(NH_3)CuOCu(NH_3)]^{2+}$ dimer in the supercage.

making this complex less stable and prone to high reactivity. Above 550–600 K, the release of the last NH_3 could disrupt the complex, and Cu ions located at site III would then migrate to site II. This could explain the decrease in SCR activity observed between 550 and 600 K (Fig. 8).

There are two N_2O formations on Cu(76)-FAU depending on the reaction temperature (Fig. 8B). The first occurring in the range 450–550 K culminates at 8% selectivity and might be assigned to traces of CuO aggregates present in the catalyst. The volcano-shaped profile of N_2O selectivity with a maximum at 500 K looks indeed like that exhibited by Cu(195)/FAU which contains 80% of Cu as CuO (Fig. 7B).

In contrast, CuO aggregates cannot be charged for the formation of N_2O above 600 K. This formation exists on Cu(56)- and Cu(37)-FAU as well. Nevertheless, the N_2O yield at full NO conversion clearly decreases from 350 ppm on Cu(76)-FAU to 200 ppm on Cu(56)-FAU and 100 ppm on Cu(37)-FAU (Fig. 8B). As for the SCR activity at 500 K, the N_2O formation at high temperature is boosted by the increase in Cu content. In line with the previous comments several neighbor Cu ions seem necessary for the formation of N_2O. At 600 K, there is no more NH_3 ligand bonded to Cu, which in the supercage can thereby occupy site II only. The separation of sites II in supercages is larger than 0.7 nm and the involvement of two Cu ions in the same active sites can hardly be conceived. On the contrary, the formation in sodalite cavities of a Cu ion pair, bridge-bonded by O^{2-}, has been proposed (28, 47–49). We may postulate that N_2O is formed on a Cu ion pair, like $[CuOCu]^{2+}$ dimer species, located in the sodalite cavities. In SCR experiments at 750 K with $^{14}NH_3/^{15}NH_3$ switches, the only occurrence of $^{14}N^{15}NO$, with traces of $^{15}N_2O$, provides evidence that N_2O is selectively formed from reaction of NO with NH_3.

CONCLUSIONS

We have demonstrated that Cu-exchanged FAU catalysts are very efficient for the SCR of NO by NH_3 in the presence of O_2. Several points of this study can be highlighted:

1. The SCR obeys the $Cu^{2+} \leftrightarrow Cu^{+}$ redox cycle, in which Cu^{2+} is reduced by $NO + NH_3$ to Cu^{+}, which in turn is oxidized to Cu^{2+} by $NO + O_2$. The oxidation of Cu^{+} by O_2 alone might compete above 650 K.

2. The original feature of the process concerns the oxidation of Cu^{+} which is much faster by $NO + O_2$ than by O_2. This point clearly differentiates from the SCR on V_2O_5/TiO_2, where V^{4+} is oxidized back to V^{5+} by O_2 alone. This behavior leads to a NH_3/NO stoichiometry lower than unity in the overall SCR reaction, of 0.77 below 550 K and 0.86 above 600 K.

3. The active sites below 550 K are formed by Cu ions in close vicinity, maybe $[CuOCu]^{2+}$, stabilized by NH_3 and located in the supercages. Above 600 K, all Cu ions become active.

4. There are two modes of N_2O formation: on residual CuO aggregates, centered at ca. 540 K; at high temperature (>650 K) on neighboring Cu ions located in the sodalite cavities.

ACKNOWLEDGMENT

This work was supported by Grande Paroisse/ATO, in the form of a grant and scholarship to Stéphane Kieger.

REFERENCES

1. Bosch, H., and Janssen, F., *Catal. Today* **2**, 369 (1988).
2. Forzatti, P., and Lietti, L., *Heterogeneous Chem. Rev.* **3**, 33 (1996).
3. Topsøe, N.-Y., *CatTech* 125 (1997).
4. Byrne, J. W., U.S. Patent No. 4,961,917 (1990).
5. Kiovsky, J. R., Koradia, P. B., and Lim, C. T., *Ind. Eng. Chem. Prod. Res. Dev.* **19**, 218 (1990).
6. (a) Descat, G., and Hamon, C., U.S. Patent No. 5,369,070 (1994); (b) Descat, G., and Hamon, C., U.S. Patent No. 5,536,483 (1996).
7. Topsøe, N.-Y., *Science* **265**, 1217 (1994).
8. Mizumoto, M., Yamazoe, N., and Seiyama, T., *J. Catal.* **59**, 319 (1979).
9. Komatsu, T., Nunokawa, M., Moon, I. S., Takahara, T., Namba, S., and Yashima, T., *J. Catal.* **148**, 427 (1994).
10. Brandin, J. G. M., Andersson, L. A. H., and Odenbrand, C. U. I., *Catal. Today* **4**, 187 (1989).
11. Ham, S. W., Choi, H., Nam, I. S., and Kim, Y. G., *Catal. Lett.* **42**, 35 (1996).
12. Williamson, W. B., and Lunsford, J. H., *J. Phys. Chem.* **80**, 2664 (1976).
13. Mizumoto, M., Yamazoe, N., and Seiyama, T., *J. Catal.* **55**, 119 (1978).
14. Wang, W., and Hwang, S., *Appl. Catal. B* **5**, 187 (1995).
15. Komatsu, T., Ogawa, T., and Yashima., *J. Phys. Chem.* **99**, 13053 (1995).
16. Choi, E. Y., Nam, I. S., and Kim, Y. G., *J. Catal.* **161**, 597 (1996).
17. Internal note from nitric plant of the Grande Paroisse Society.
18. Lemaitre, J. L., *in* "Characterization of Heterogeneous Catalysts" (F. Delannay, Ed.), p. 34. Marcel Dekker, New York, 1984.
19. Tanabe, S., and Matsumoto, H., *Chem. Lett.*, 1425 (1985).
20. Schoonheydt, R. A., *Catal. Rev.-Sci. Eng.* **35**, 129 (1993).
21. Shimokawabe, M., Asakawa, H., and Takezawa, N., *Appl. Catal.* **59**, 45 (1990).
22. Centi, G., Perathoner, S., Biglino, D., and Giamello, E., *J. Catal.* **151**, 75 (1995).
23. Herman, R. G., Lunsford, J. H., Beyer, H., Jacobs, P. A., and Uytterhoeven, J. B., *J. Phys. Chem.* **79**, 2388 (1975).
24. Jacobs, P. A., Linart, J.-P., Nijs, H., and Uytterhoeven, J. B., *J. Chem. Soc. Faraday Trans. 1* **73**, 1745 (1977).
25. Gentry, S. J., Hurst, N. W., and Jones, A., *J. Chem. Soc. Faraday Trans. 1* **73**, 1688 (1979).
26. Robertson, S. D., McNicol, B. D., de Baas, J. H., Cloet, S. C., and Jenkins, J. W., *J. Catal.* **37**, 424 (1975).
27. Delk, F. S., and Vavere, A., *J. Catal.* **85**, 380 (1984).
28. Jacobs, P. A., de Wilde, W., Schoonheydt, R. A., Uytterhoeven, J. B., and Beyer, H., *J. Chem. Soc. Faraday Trans. 1* **72**, 1221 (1976).
29. Datka, J., Gil, B., and Kubacka, A., *Zeolites* **15**, 501 (1995).
30. Baranski, A., Dal, T., and Galuszka, J., *Bull. Acad. Pol. Sci.* **27**, 363 (1979).
31. Howard, J., and Nicol, J. M., *J. Chem. Soc. Faraday Trans. 1* **85**, 1233 (1989).
32. Flentge, D. R., Lunsford, J. H., Jacobs, P. A., and Uytterhoeven, J. B., *J. Phys. Chem.* **79**, 354 (1975).
33. Huang, Y., and Vansant, E. F., *J. Phys. Chem.* **77**, 663 (1973).
34. Vansant, E. F., and Lunsford, J. H., *J. Phys. Chem.* **76**, 2860 (1972).

35. Li, Y., and Armor, J. N., *Appl. Catal.* **76**, L1 (1991).
36. Coq, B., Tachon, D., Figuéras, F., Mabilon, G., and Prigent, M., *Appl. Catal. B* **6**, 271 (1995).
37. Iizuka, T., Ikeda, H., and Okazaki, S., *J. Chem. Soc. Faraday Trans. 1* **82**, 61 (1986).
38. Suzuki, M., Tsutsumi, K., Takahashi, H., and Saito, Y., *Zeolites* **8**, 98 (1989).
39. Maxwell, I. E., and de Boer, J. J., *J. Phys. Chem.* **79**, 1874 (1975).
40. Marti, J., Soria, J., and Cano, F. H., *J. Phys. Chem.* **80**, 1776 (1976).
41. Gallezot, P., ben Taarit, Y., and Imelik, B., *C. R. Acad. Sci. Paris* **272**, 261 (1971).
42. Larsen, S. C., Aylor, A., Bell, A. T., and Reimer, J. A., *J. Phys. Chem.* **98**, 11533 (1994).
43. Szanyi, J., and Paffett, M. T., *J. Catal.* **164**, 232 (1996).
44. Centi, G., and Perathoner, S., *Catal. Today* **29**, 117 (1996).
45. Delahay, G., Kieger, S., Neveu, B., and Coq, B., *C. R. Acad. Sci. Paris*, 229 (1998).
46. Iwamoto, M., Yahiro, H., Tanda, K., Mizuno, M., Mine, Y., and Kagawa, S., *J. Phys. Chem.* **95**, 3727 (1991).
47. Naccache, C. M., and Ben Taarit, Y., *J. Catal.* **22**, 171 (1971).
48. Chao, C.-C., and Lunsford, J. H., *J. Chem. Phys.* **57**, 2890 (1972).
49. Conesa, J. C., and Soria, J., *J. Chem. Soc. Faraday Trans. 1* **75**, 406 (1979).